Mesoscopic Lattice Boltzmann Modeling of Flowing Soft Systems

Roberto Benzi
University of Tor Vergata and INFN, via della Ricerca Scientifica 1, 00133 Rome, Italy

Sergio Chibbaro
Department of Mechanical Engineering, University of "Tor Vergata", via del Politecnico 1 00133, Rome, Italy

Sauro Succi
Istituto Applicazioni Calcolo, CNR, V.le del Policlinico 137, 00161, Rome, Italy
(Received 8 August 2008; published 16 January 2009)

A mesoscopic multicomponent lattice Boltzmann model with short-range repulsion between different species and short (midranged) attractive (repulsive) interactions between like molecules is introduced. The interplay between these composite interactions gives rise to a rich configurational dynamics of the density field, exhibiting many features of disordered liquid dispersions (microemulsions) and soft-glassy materials, such as long-time relaxation due to caging effects, anomalous enhanced viscosity, aging effects under moderate shear and flow above a critical shear rate.

DOI: 10.1103/PhysRevLett.102.026002 PACS numbers: 83.10.−y, 47.11.−j, 47.57.−s, 82.70.−y

The rheology of flowing soft systems, such as emulsions, foams, gels, slurries, colloidal glasses and related fluids, exhibits a number of distinctive features, such as long-time relaxation, anomalous viscosity, aging behavior, whose quantitative description requires profound extensions of nonequilibrium statistical mechanics [1]. The study of these phenomena sets a pressing challenge for computer simulation as well, since characteristic time lengths of disordered fluids can escalade tens of decades over the molecular time scales. To date, the most credited techniques for computational studies of these complex flowing materials are molecular dynamics (MD) and Monte Carlo (MC) simulations [2]. Molecular dynamics in principle provides a fully *ab initio* description of the system, but it is limited to space-time scales significantly shorter than experimental ones. Monte Carlo methods are less affected by these limitations, but they are bound to deal with equilibrium states. As a result, neither MD nor MC simulations can easily take into account the nonequilibrium dynamics of complex flowing materials on space-time scales of hydrodynamic interest. In the last decade, a powerful mesoscopic technique, based on minimal lattice formulations of Boltzmann's kinetic equation, has been developed for ideal and complex fluids [3,4]. In the latter, potential energy interactions are represented through a density-dependent mean-field pseudopotential, $\Psi[\rho]$, and phase separation is achieved by imposing a short range attraction between the light and dense phases. In this Letter, we provide the first numerical evidence that a suitably extended, two-species, mesoscopic lattice Boltzmann model, is capable of reproducing many features of soft-glassy materials (microemulsions), such as structural arrest, anomalous viscosity, cage-effects and aging under shear. The key feature of our model is the capability to investigate the rheology of these systems on space-time scales of hydrodynamic interest at an affordable computational cost.

The kinetic lattice Boltzmann equation takes the following form [3]:

$$f_{is}(\vec{r}+\vec{c}_i, t+\Delta t) - f_{is}(\vec{r}, t) = -\frac{\Delta t}{\tau_s}[f_{is}(\vec{r}, t) - f_{is}^{(\mathrm{eq})}(\vec{r}, t)] + F_{is}\Delta t, \tag{1}$$

where f_{is} is the probability of finding a particle of species s at site $\vec{r}$ and time t, moving along the ith lattice direction defined by the discrete speeds $\vec{c}_i$ with $i = 0, \ldots, b$. The left-hand side of (1) stands for molecular free-streaming, whereas the right-hand side represents the time relaxation (due to collisions) towards local Maxwellian equilibrium on a time scale τ_s and F_{is} represents the volumetric body force due to intermolecular (pseudo)-potential interactions. The pseudopotential force within each species consists of an attractive component, acting only on the first Brillouin region (belt, for simplicity), and a repulsive one acting on both belts, whereas the force between species is short-ranged and repulsive: $\vec{F}(\vec{r}, t) = \vec{F}_s^a(\vec{r}, t) + \vec{F}_s^r(\vec{r}, t) + \vec{F}_s^X$, where

$$\begin{aligned}
\vec{F}_s^a(\vec{r}, t) &= G_s^a \Psi_s(\vec{r}; t) \sum_{i=0}^{b_1} w_i \Psi_s(\vec{r}_{1i}, t)\vec{c}_{1i}\Delta t, \\
\vec{F}_s^r(\vec{r}, t) &= G_s^r \Psi_s(\vec{r}; t) \sum_{i=0}^{b_1} p_{1i} \Psi_s(\vec{r}_{1i}, t)\vec{c}_{1i}\Delta t \\
&\quad + G_s^r \Psi_s(\vec{r}; t) \sum_{i=1}^{b_2} p_{2i} \Psi_s(\vec{r}_{2i}, t)\vec{c}_{2i}\Delta t, \\
\vec{F}_s^X(\vec{r}_i; t) &= \frac{G_{AB}}{\rho_0} \rho_s(\vec{r}; t) \sum_{i=0}^{b_1} w_i \rho_{s'}(\vec{r}_i; t)\vec{c}_i \Delta t.
\end{aligned} \tag{2}$$

In the above, the indices $k = 1, 2$ refer to the first and

second Brillouin zones in the lattice, $\vec{c}_{ki}$, p_{ki}, w_i are the corresponding discrete speeds and associated weights. In the above, $G_{AB} \equiv G_{ss'} = G_{s's}$, $s' \neq s$, is the cross coupling between species, ρ_0 a reference density to be defined shortly and, finally, $\vec{r}_{ki} \equiv \vec{r} + \vec{c}_{ki}\Delta t$ are the displacements along the ith direction in the kth belt and ρ_0 marks the density value at which nonideal effects come into play. These interactions are sketched in Fig. 1. Following [5], Taylor expansion of (2) to fourth order in Δt delivers the nonideal pressure tensor $P_{\alpha\beta}(\vec{r}; t)$, namely,

$$P_{\alpha\beta} = \left[c_s^2\rho_A + c_s^2\rho_B + \tfrac{1}{2}c_s^2 G_{A1}\Psi_A^2 + \tfrac{1}{2}c_s^2 G_{B1}\Psi_B^2 + c_s^2\frac{G_{AB}}{\rho_0}\rho_A\rho_B + c_s^4\Pi\right]\delta_{\alpha\beta} - c_s^4\gamma_{\alpha\beta}, \quad (3)$$

where greek indices run over spatial dimensions, and

$$\Pi = \Sigma_{s=A,B}G_{s2}\left[\frac{1}{4}(\nabla\Psi_s)^2 - \frac{1}{2}\Psi_s\Delta\Psi_s\right] + \frac{G_{AB}}{\rho_0}[\rho_A\Delta\rho_B + \rho_B\Delta\rho_A - \nabla\rho_A\nabla\rho_B], \quad (4)$$

$$\gamma_{\alpha\beta} = \Sigma_{s=A,B}G_{s2}\partial_\alpha\Psi_s\partial_\beta\Psi_s + \frac{G_{AB}}{2\rho_0}(\partial_\alpha\rho_A\partial_\beta\rho_B + \partial_\alpha\rho_B\partial_\beta\rho_A). \quad (5)$$

In the above equations, we have introduced the effective couplings $G_{s1} = G_s^a + G_s^r$ and $G_{s2} = G_s^a + \frac{12}{7}G_s^r$, $s = A$, B, respectively. The nonideal pressure splits into a local (bulk) and nonlocal (surface) contributions, which fix the surface tension σ of the model. It is worth noting that, once all the couplings are fixed, the value of σ can be tuned by changing the reference density ρ_0. The repulsive intraspecies force $\vec{F}_s^r$ acts against the interspecies repulsive force $\vec{F}^X$ (proportional to $1/\rho_0$). Thus, for small ρ_0, $\vec{F}^X$ dominates and a complete separation between the two fluids is expected. This is the case of large and positive σ. On the other hand, for large ρ_0, σ becomes smaller and even negative, see Fig. 2(a). Full details of the model are given in [6]. Next, we discuss numerical simulations with random initial conditions for the two densities ρ_A and ρ_B. More specifically, we choose $\langle\rho_A\rangle = \langle\rho_B\rangle = 0.612$, with a standard deviation $\sigma_d = 0.01$. The set of parameters has been chosen in such a way as to fulfill two physical conditions: (i) both components A and B are away from phase-transition; (ii) realize a surface tension of order $\sigma \sim 0.01$ (lattice units), corresponding to a physical value below $10^{-4}N$, as it is appropriate for microemulsions. After a short transient, the interfacial area reaches its maximum value and progressively tends to decrease due to the effect of surface tension. In the long term, this minimum-area tendency would lead to the complete separation between components A and B, with a single interface between two separate bulk components. However, such a tendency is frustrated (hence, strongly retarded) by the complex interplay between repulsive (short-range interspecies and mid-range intraspecies) and attractive (short-range intraspecies) interactions. The final result is a rich configurational dynamics of the density field, as the one shown in Fig. 2, right

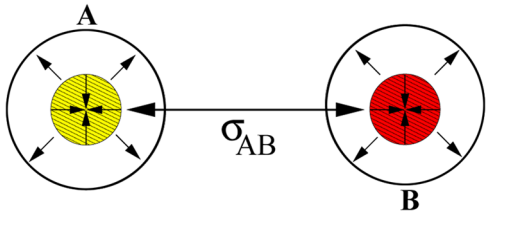

FIG. 1 (color online). The two components A and B interact via a repulsive pseudopotential, which supports a surface tension σ_{AB}. Moreover, each component experiences an attractive interaction in the first Brillouin zone and a repulsive one acting on both Brillouin zones. Each of these interactions can be tuned through a separate coupling constant.

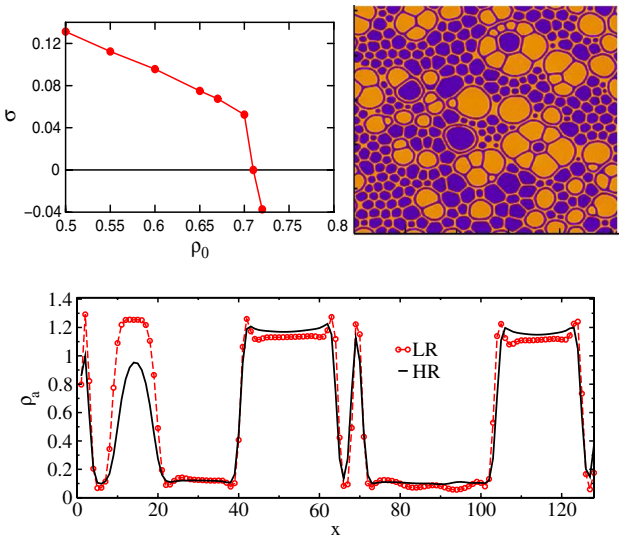

FIG. 2 (color online). The nominal surface tension of the two-component fluid as a function of the reference density ρ_0 (left panel). The coupling parameters are $G_A^a = -12.55$, $G_A^r = 11.70$, $G_B^a = -11.71$, $G_B^r = 10.95$, $G_{AB} = 0.58$. Above a critical value, $\rho_{\text{crit}} \sim 0.72$, the nominal surface tension turns negative. Right panel: A typical snapshot of the density field ρ_A at time 2×10^6 (lattice units) at resolution 512^2. Once the separation between A and B phases has occurred, we obtain $\rho_A \approx 1.2$ in the region occupied by phase A, and $\rho_A \sim 0.1$ elsewhere (the same values, although complementary in space, occur for fluid B). The interface width is $w \sim 5$ lattice points wide. A cut of the density distribution across the interface shows that the profile is not monotonic, with small bumps on both high and low-density ends (bottom panel, dashed line, open symbols, LR). To investigate the nature of these bumps, we have performed additional simulations at higher resolution (black solid line, HR), by tuning the parameters G and ρ_0 as outlined in [5] ($G_A^a = -8.2$, $G_A^r = 7.38$, $G_B^a = -7.29$, $G_B^r = 6.47$, $G_{AB} = 0.49$, $\rho_0 = 0.83$). The bumps are indeed seen to attenuate at higher resolution, which points to a numerical rather than physical origin. Because of the small but positive value of σ (for $\rho_0 = 0.7$, we find $\sigma = 0.0525$), the system proves capable of supporting fairly complex metastable density configurations.

panel. In order to investigate the rheological properties of the composite LB fluid, we put the system under a shear flow $U_x(x, y) = U_0 \sin(ky)$, with $k = 1$, $U_y = 0$, by imposing a volumetric body force constant in time, and measure the response function $R(t) = \frac{\hat{\bar{U}}(k=1;t)}{U_0} \equiv \frac{\nu_0}{\bar{\nu}}$, where $\hat{\bar{U}}(k; t)$ is the Fourier transform of the line-averaged speed along the x direction, $\bar{U}(y; t) = \sum_x U(x, y; t)/N_x$, and $\bar{\nu}$ defines the effective viscosity.

Under normal flow conditions, $R = 1$, so that $R \ll 1$ provides a direct signal of enhanced viscosity and eventually, structural arrest. The main coupling parameters are $G_A^a = -12.55$, $G_A^r = +11.80$, $G_B^a = -11.70$, $G_B^r = +10.95$, $G_{AB} = +0.58$, and $\rho_0 = 0.7$. These parameters correspond to both species in the dense phase, (no phase transition), and surface tension below 10^{-3} N/m, hence descriptive of glassy micro- or nanoemulsions. By letting each species undergo phase transitions between a dense and light phase, the same model could describe foamy materials as well. The simulations are performed mostly on a 128^2 grid (except for the one reported in Fig. 2) up to 5×10^6 LB time steps. In Fig. 3, we show the time evolution of the response $R(t)$, as well as an indicator of the interface area, $I_{AB}(t) = \sum_{x,y} \nabla\rho_A \nabla\rho_B$. From this figure, we appreciate a very dramatic drop of the flow speed in the initial stage of the evolution, corresponding to a very substantial enhancement of the fluid viscosity (about four orders). The system remains in this "arrested" state for a very long time, over three million time steps, until it suddenly starts to regain its initial velocity through a bumpy dynamics, characterized by a series of sudden jumps [7]. These viscosity jumps signal "plastic events",

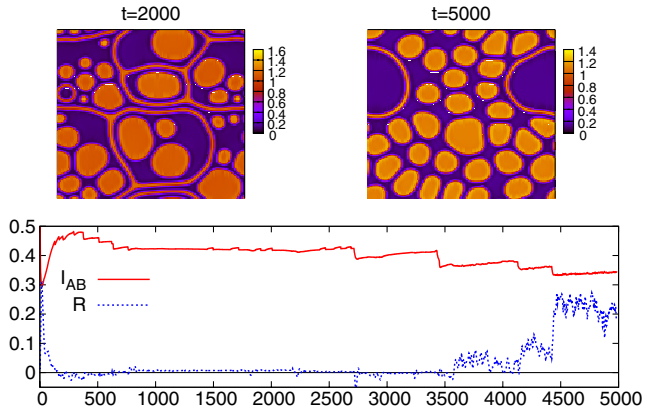

FIG. 3 (color online). The response function $R(t)$ and the surface indicator $I_{AB}(t)$ as a function of time, (expressed in units of 10^3 LB time steps). The forcing is $U_0 = 0.1$, the domain is 128^2 and the other parameters are defined in the text. The sharp decrease of the response function in the initial stage indicates the structural arrest of the system, associated with an anomalous enhancement of the flow viscosity, about 4 orders of magnitude above the molecular value. In the left panel, cages are present, which manage to "trap" microstructures inside. In the right panel, the cages break down and the system is now able to flow again.

whereby the system manages to break the density locks (cages) which blocked the flow in the initial phase. As a result, the system progressively regains its capability to flow. These plastic events are also recorded by the time trace of the interface area I_{AB}, which exhibits an alternate sequence of plateaux followed by sudden down jumps, the latter being responsible for the overall reduction of the interface area as time unfolds. Visual inspection of the fluid morphology confirms this picture. In the top panels of Fig. 3, we show the density field in an arrested state at time $t = 2 \times 10^5$ (top, left) and in a flowing state, $t = 5 \times 10^5$ (top, right). The left figure clearly reveals the existence of "cages" in the density field configuration, which entrap the fluid inside and consequently block its net macroscopic motion. Interdomain relaxation can only take place in response to "global moves" of the density field, i.e., the cage rupture. We have also performed additional simulations (not shown for space limitations) to investigate the robustness of the response function $R(t)$ towards changes in the initial conditions. Consistently with the glassy nature of the system, the plateau location is found to exhibit a strong sensitivity to the noise realization in the initial conditions, with some realizations showing early onset of structural arrest (a few hundreds of thousands time steps), and others spending nearly the entire simulation time-span (up to five millions of time steps) without entering the arrested state. Because of the mesoscopic nature of the present model, the rupture of a single cage in the LB simulation corresponds to a large collection of atomistic ruptures, and, consequently, it leads to observable effects in terms of structural arrest of the system. To the best of our knowledge, this the first time that such an effect is observed by means of a mesoscopic lattice Boltzmann model. To be noted that the use of high-order lattices (24 speeds) is instrumental to this program, since, by securing the isotropy of lattice tensors up to 8th order, such lattice permits to minimize spurious effects on the nonideal hydrodynamic forces acting upon the discrete lattice fluid [5]. We next inspect another typical phenomenon of soft-glassy matter, namely, ageing. To this purpose, following upon the spin-glass literature [8], we define the order parameter $\phi \equiv (\rho_A - \rho_B)$ and compute its *overlap*, defined through the autocorrelation function:

$$C(t_w, \tau) = \frac{\langle \sum_{x,y} \phi(x, y; t_w)\phi(x, y; t_w + \tau)\rangle}{\langle \sum_{x,y} \phi(x, y; t_w)\phi(x, y; t_w)\rangle}, \qquad (6)$$

where t_w is the waiting time, τ is the time lapse between the two density configurations and brackets stand for averaging over an ensemble of realizations. In Fig. 4, we show the correlation function corresponding to different waiting times t_w ($t_w = 5 \times 10^4$, red, squares; $t_w = 2 \times 10^5$, green, circles; and $t_w = 3 \times 10^5$, blue, triangles) for shear stress $U_0 = 0.02$. Aging effects are clearly visible, in the form of a slower than exponential decay of the correlation function, which saturates to a nonzero value in the long-time limit (broken ergodicity). In the inset of the same figure, we

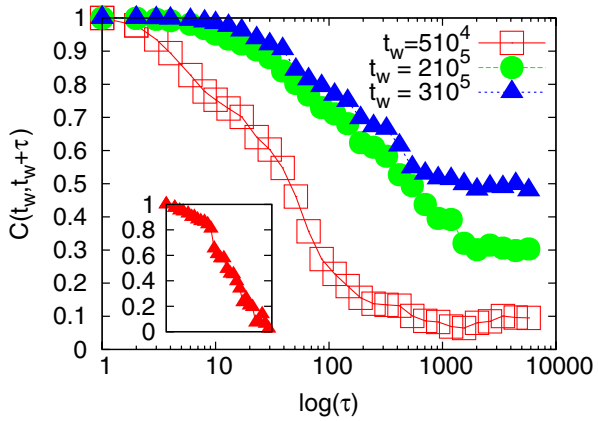

FIG. 4 (color online). Aging of the system. Correlation function corresponding to different waiting times t_w ($t_w = 5 \times 10^4$, red, squares; $t_w = 2 \times 10^5$, green, circles; and $t_w = 3 \times 10^5$, blue, triangles) with shear stress $U_0 = 0.02$. In the inset, we show the correlation function for $t_w = 3 \times 10^5$ and $U_0 = 0.03$: with increasing shear stress the structural arrest disappears.

show the correlation function for $t_w = 3 \times 10^5$ and $U_0 = 0.03$: with increasing shear stress the structural arrest disappears, which is one of the most distinctive features of flowing soft-glassy materials [9]. The main advantage of the present lattice mesoscopic approach is to give access to hydrodynamic scales at an affordable computational cost. With reference to microemulsions (say water and oil), we note that the presence of surfactants usually gives rise to microscopic structures of the order of 50 nm in size [10]. These can be likened to the "blobs" observed in our simulations. With reference to liquid water, we have $\nu \sim 10^{-6}$ (m^2/s), which provide a physical measure of the time step $\Delta t \sim 4$ ps, about 3 orders of magnitude larger than the typical time step used in molecular dynamics. As a result, a five-million time-step LB simulation spans about 20 μs in physical time. Since the present LB method is easily amenable to parallel computing, parallel implementations will permit to track the time evolution of three-dimensional microemulsions of tens of microns in size, over time spans close to the millisecond, i.e., at space-time scales of hydrodynamic relevance. Summarizing, we have provided the first numerical evidence that a two-species mesoscopic lattice Boltzmann model with midrange repulsion between like molecules and short-range repulsion between different ones, is capable of reproducing many distinctive features of soft material behavior, such as slow relaxation, anomalous enhanced viscosity, caging effects, and aging under shear. The present lattice kinetic model caters for this very rich physical picture at a computational cost only marginally exceeding the one for a simple fluid. As a result, it is hoped that it can be used as an alternative or complement to Monte Carlo calculations and/or molecular dynamics, for future investigations of the *nonequilibrium* rheology of a broad class of flowing disordered materials, such as microemulsions, foams, and slurries on space and time scales of experimental interest. For a better comparison with experiments and other models [10], we are currently working at deriving an explicit free-energy functional corresponding to the phenomenological equations (2)–(5).

S. S. wishes to acknowledge financial support from the project INFLUS (NMP3-CT-2006-031980) and SC financial support from the ERG EU grant and consorzio COMETA. Fruitful discussions with L. Biferale, M. Cates, D. Nelson, G. Parisi, M. Sbragaglia, and F. Toschi are kindly acknowledged. The authors are thankful to A. Cavagna for a critical reading of this manuscript.

[1] W. B. Russel, D. A. Saville, and W. R. Schowalter, *Colloidal Dispersion* (Cambridge University Press, Cambridge England, 1989); P. H. Poole, F. Sciortino, U. Essmann, and H. E. Stanley, Nature (London) **360**, 324 (1992); P. Sollich, F. Lequeux, P. Hébraud, and M. E. Cates, Phys. Rev. Lett. **78**, 2020 (1997); R. G. Larson, *The Structure and Rheology of Complex Fluids* (Oxford University Press, New York, 1999); T. Eckert and E. Bartsh, Phys. Rev. Lett. **89**, 125701 (2002); K. N. Pham *et al.*, Science **296**, 104 (2002); H. Guo *et al.*, Phys. Rev. E **75**, 041401 (2007); P. Schall *et al.*, Science **318**, 1895 (2007); P. J. Lu, E. Zaccarelli, F. Ciulla, A. B. Schofield, F. Sciortino, and D. A. Weitz, Nature (London) **453**, 499 (2008).

[2] M. P. Allen, and D. J. Tildesley, *Computer simulations of liquids* (Oxford University Press, New York, 1990). D. Frankel and B. Smith, *Understanding Molecular Simulation* (Academic Press, San Diego, 1996). K. Binder and D. W. Herrman *Monte Carlo Simulation in Statistical Physics* (Springer, Berlin, 1997). W. Kob in *Slow Relaxation and Nonequilibrium Dynamics in Condensed Matter*, edited by J.-L. Barrat, M. Feigelman, and J. Kurchan (Springer, Berlin, 2003).

[3] R. Benzi, S. Succi, and M. Vergassola, Phys. Rep. **222**, 145 (1992); S. Chen and G. D. Doolen, Annu. Rev. Fluid Mech. **30**, 329 (1998).

[4] X. Shan and H. Chen, Phys. Rev. E **47**, 1815 (1993).

[5] M. Sbragaglia, R. Benzi, L. Biferale, S. Succi, K. Sugiyama, and F. Toschi, Phys. Rev. E **75**, 026702 (2007).

[6] S. Chibbaro, G. Falcucci, X. Shan, H. Chen, and S. Succi, Phys. Rev. E **77**, 036705 (2008).

[7] G. J. Papakonstantopoulos, R. A. Riggleman, J.-L. Barrat, and J. de Pablo, Phys. Rev. E **77**, 041502 (2008).

[8] G. Biroli, J.-P. Bouchaud, A. Cavagna, T. S. Grigera, and P. Verrocchio, arXiv:0805.4427v1.

[9] P. Coussot *et al.*, Phys. Rev. Lett. **88**, 218301 (2002); L. Buisson, A. Garcimartin, and S. Ciliberto, Europhys. Lett. **63**, 603 (2003).

[10] S. Wu, H. Westfahl, Jr., J. Schmalian, and P. G. Wolynes, Chem. Phys. Lett. **359**, 1 (2002); S. Wu,J. Schmalian, G. Kotliar, and P. G. Wolynes, Phys. Rev. B **70**, 024207 (2004).